Electrodynamics at rough metal surfaces: Photochemistry and luminescence of adsorbates near metal-island films

S. Garoff, D. A. Weitz, M. S. Alvarez, and J. I. Gersten[a)]
Exxon Research and Engineering Company, Annandale, New Jersey 08801

(Received 4 May 1984; accepted 2 August 1984)

Detailed measurements of the photochemical and photophysical properties of an adsorbate on discontinuous metal-island films are used to explore the unusual electrodynamics near rough metal surfaces. Several aspects of the properties have been measured: the magnitude, the temporal decay of the fluorescence, the shape and temporal evolution of the fluorescence spectrum, and the effects on the spectrum of a photochemical hole-burning process. Dramatic increases in the fluorescent decay rate and decreases in the photochemical reaction rate as well as systematic spectral shifts of the emission of molecules experiencing the different electrodynamic environments on the island film are observed. These results reveal the strong effects of the coupling between the adsorbate and the plasma resonances localized on the islands of the film. We model our results using the electrodynamic picture which has successfully described many aspects of surface-enhanced Raman scattering and other optical processes on island films. The excellent agreement between this model and our results suggests that an important feature of the electrodynamics at these rough metal surfaces is the dipolar character of the couplings between the surface, the adsorbate, and the optical fields.

I. INTRODUCTION

The observation of surface-enhanced Raman scattering (SERS)[1] has stimulated considerable interest and effort in the investigation of the optical properties of molecules adsorbed to rough metal surfaces. In addition to the large increase in the Raman scattering cross section, profound surface-induced effects on the adsorbates are also observed for absorption,[2,3] resonance Raman scattering,[4] fluorescence,[5–8] photochemical reaction rates,[9,10] and a variety of nonlinear optical effects.[11–13] There remains some controversy over the detailed contributions of a variety of mechanisms which lead to these surface-induced optical effects. Nevertheless, there is a general consensus that electrodynamic interactions among the optical fields, the vibrational and electronic states of the adsorbate, and the plasma resonances of the rough surface play a major, and often dominant, role in the origin of these phenomena. A generalized model based on these interactions[14,15] has been used to obtain a unified account of the observed enhancements of normal Raman scattering, resonance Raman scattering and fluorescence,[4] the excitation profile of Raman scattering,[16] fluorescent lifetimes,[7] and photochemical reaction rates.[9]

In this paper, we describe detailed measurements of the photochemical and photophysical properties of an adsorbate on discontinuous metal-island films. We focus on "delayed" processes, those occurring after dephasing and thermalization of the excited state of the adsorbate. Our goal is to present a comprehensive set of experimental results complemented by a unified analysis of all our observations. We measure the temporal decay of the fluorescent emission, the rate of the photochemically induced degradation of the adsorbate, as well as the shape of the fluorescent emission (a) on different types of island films, (b) before and after photochemical degradation, and (c) as a function of time after pulsed excitation. We use the same adsorbate, Ruthenium tris-bipyridine (RuTBP), in all our measurements. Our surfaces are island films which are optically well characterized.[16] The discontinuous structure of these films creates an inherent variation in distances between adsorbates and roughness features of the surface. We exploit this structure to probe the distance dependence of the electrodynamic interactions. Our measurements show that molecules nearest islands on the film have emission properties most severely altered compared to their properties in an electromagnetically inert environment. Their emission rate is dramatically increased; their photochemical degradation rate is dramatically decreased; and their spectra are significantly shifted. The observation of these changes allows us to probe the spatial dependence of the electrodynamic couplings and thus the inhomogeneities in the environment of the island films. The temporal and spectral behavior complement each other in probing the spatial dependence. All these results are interpreted in a consistent fashion within the framework of the electrodynamic couplings with the details of the molecular resonance and the relaxed emission process included. Thus, they provide a detailed picture of the consequences of the electrodynamic interactions on the delayed emission and photochemistry of the adsorbates. Particularly intriguing are the spectral shifts of the emission from molecules most strongly coupled to islands. These shifts originate from the strong interaction between the island and the vibronic structure of the electronic state manifolds of the adsorbed molecules.

In the next section, we describe the experimental procedures, while in Sec. III, we discuss the results and interpret them within the electrodynamic framework. The final section summarizes our work, and the Appendix presents the detailed derivation of our expressions for the temporal decay of fluorescence of molecules on island films.

[a)] Physics Department, City College of the City University of New York, New York, New York 10031.

 0021-9606/84/235189-12$02.10

II. EXERIMENTAL PROCEDURES

Silver-island films are produced on silica and thermally oxidized aluminum by evaporation of silver at a base pressure of 10^{-6} Torr. The silver is deposited at ~ 1 Å/s to a mass thickness of 50 Å. The substrate temperature is maintained at 150 °C during the evaporation.[17] As shown by electron microscopy, the films are composed of roughly circular islands ~ 200 Å in diameter and separated by distances comparable to their diameter. This island morphology leads to an optical absorption resonance peaking at ~ 435 nm and with a full width at half-maximum of ~ 140 nm. This absorption behavior is characteristic of the plasma resonances occurring on these films.[18] Normal Raman scattering from adsorbates on these films is enhanced by about 10^5, and the excitation profile for the Raman scattering is described by the electrodynamic model for SERS.[16] Reflectivity studies show that the plasma resonance remains for island films on the aluminum substrates. Gold-island films are made in a similar fashion and have qualitatively similar structure and characteristics except that the absorption resonance of the films is shifted to ~ 560 nm with a full width at half-maximum of ~ 160 nm.

Submonolayer coverages of RuTBP are applied by a dipping technique which produces approximately equal molecular coverages independent of the substrate.[19] RuTBP in solution has a broad absorption profile in the visible which is roughly coincident with the absorption resonance of the silver-island film. The emission spectrum in solution is also broad with a peak at ~ 630 nm[20] and the quantum yield in some solvents approaches 10%.[21] Coverages of RuTBP on all substrates is low enough that the absorption spectra of the coated island films indicate that the electromagnetic resonances of the film are not measurably altered by the coating.[2] Surface coverages are also low enough that concentration quenching of fluorescence due to surface dimer formation is not present.[19]

All emission spectra are measured using 457.9 or 488.0 nm excitation with low power density (~ 0.1 W/cm^2) and a spinning sample. These precautions prevent photochemical degradation of the sample during the aquisition of spectra. Photodegradation of the sample is induced by increasing the laser power by a factor of 10 and stopping the spinning of the sample.

The temporal decay of the intensity of fluorescent emission as well as the temporal development of the emission spectrum are measured by photon correlation methods.[22] Briefly, the times of arrival of the laser pulse at a fast photodiode and of the first photon emitted from the sample at the photomultiplier of the spectrometer are marked by timing pulses generated by constant fraction discriminators. These pulses form a start and stop pulse pair for a time-to-amplitude (TAC) converter which generates a pulse whose amplitude is proportional to the time difference. A pulse height analyzer then forms a histogram of the number of these pulses vs time between start/stop pulse pairs. This histogram represents the fluorescent decay curve of the sample. These decay curves are obtained at a fixed wavelength of the emission monochromator. The laser pulses were generated by a mode-locked, cavity-dumped Ar^+ laser and were ~ 200 ps full width at half-maximum. However, the temporal resolution of the experiments was limited by the spread in transit times of the photoelectrons of the phototube giving the apparatus a response to delta function excitation of 600 ps full width at half-maximum. Thus, times shorter than 1 ns cannot be resolved.

Temporally resolved spectra are measured using a variation of a technique which has been suggested for fluorescence rejection for Raman spectroscopy.[23] The apparatus is essentially the same as that used to measure lifetimes. However, the output of the TAC is now fed into a single channel analyzer (SCA) which generates a pulse only if the TAC output is between two preset amplitude levels. Thus, the count rate of the SCA represents the number of photons per second emitted from the sample in a specific time interval after laser excitation. If the monochromator of the spectrometer is now scanned with the SCA settings fixed, a spectrum of the emission at a fixed delay after excitation is generated. The spectrum may then be generated at different delay times.

III. RESULTS AND DISCUSSION

The details of the electrodynamic interactions between the adsorbates and the electronic plasma resonances of a metal spheroid are by now well known[4,14,15] and will not be presented here. Instead, in Sec. III A, we present a brief overview of the essential physics of these interactions. Further details of the electrodynamic model as applied to delayed optical processes on island films are presented in the Appendix of this paper.

In the experiments discussed in this paper, the fluorescent emission from adsorbates on island films is used as a direct probe of the delicate balance of the various surface-induced electrodynamic processes. In particular, the experiments focus on the dependence of the balance on the distance of the adsorbate from the island. As discussed in Sec. III B, the measurements of the intensities and lifetimes of fluorescence and the photochemical reaction rates provide an explicit demonstration of the shortening of the decay times of excited states of the adsorbate on the film. The measurements of the full temporal decay of the fluorescence are used to examine the dependence of decay rates on molecule-island separation. This is described in Sec. III C. Finally, in Sec. III D, we describe some important consequences of the electrodynamic interactions by probing the systematic variations in the shape of the fluorescent emission spectrum (a) of different types of island films, (b) before and after photochemical degradation, and (c) as a function of time after pulsed excitation.

A. Overview of electrodynamics

The electrodyamic coupling among the optical fields, the electronic and vibrational states of the adsorbate, and the localized plasma resonances of the metal islands of the film are modeled using semiclassical radiation theory. The islands are considered to be spheroidal; and since they are much smaller than the optical wavelengths, their response is assumed to be dominantly dipolar. The dipolar character of the response of the island is the essential feature of the electrodynamics which leads to the observed optical effects.

The local fields in and around the islands are enhanced due to coupling between plasma resonances in the island and the incoming optical wave. We can represent the local field enhancement by a complex valued function

$$A(\omega,r) = 1 + \frac{2\beta(\omega)}{r^3}, \tag{1}$$

where ω is the frequency of the incoming plane wave and r is the separation between the molecule and the center of the island. $\beta(\omega)$ is the effective polarizability of the island which becomes large at the frequency of the plasma resonance. (The precise functional form of A and other quantities discussed in the section depend on molecular orientation. The details of this dependence may be found in the Appendix.)

In addition to the enhancement of local fields, the electrodynamic coupling also causes the oscillating dipole of the excited molecule to induce a response in the island. The emission dipole of the coupled system is larger than the molecular dipole by the same amplification factor $A(\omega',r)$, which accounts for local field amplification except the factor is now evaluated at the emission frequency ω'. The radiative decay rate, which is proportional to the square of the emission dipole, is therefore increased by the electrodynamic coupling. The out-of-phase component of the induced dipole leads to damping of the energy of the system. This out-of-phase dipolar component as well as higher order multipolar components lead to new nonradiative decay pathways further decreasing the lifetime of the adsorbate excited state. The nonradiative decay will in fact dominate in the limit of adsorbates so close to the island surface that the surface is effectively flat. Here, the decay modes of the adsorbate approach those of a molecule near a flat surface where radiation is completely quenched.[24] The total decay rate of the excited state of the system may now be written

$$\Gamma' = \gamma'_{nr} + \gamma'_{pc} + \gamma'_r |A(\omega',r)|^2 + \frac{2|\mu'_0|^2}{r^6} \operatorname{Im}\beta', \tag{2}$$

where γ'_{nr}, γ'_{pc}, γ'_r are the nonradiative, photochemical, and radiative decay rates of the free molecule, respectively and μ'_0 is its transition moment. Primed quantities are evaluated at ω' while unprimed quantities are evaluated at ω. The third term in Eq. (2) is the surface-induced increase of the radiative decay rate; while the fourth term is the additional nonradiative decay channel open to the molecule due to the out-of-plane dipolar response of the island.

These two effects produced by the electrodynamic couplings lead to the changes observed in the optical processes of molecules adsorbed near an island. The enhancement of the local incoming field leads to increased pumping rates of any optical process; while the increased decay rate leads to broadening of the excitation level of the molecular manifold of states and therefore a mitigation of the increased pumping rate. Thus the probability of absorption of a photon by the system $\langle P \rangle$ is

$$\langle P \rangle \sim \frac{|A(\omega,r)|^2}{\Gamma}. \tag{3}$$

Further, for any "delayed" optical process, the relative rates of the surface-induced radiative and nonradiative decays of the excited state can alter the emission and photochemical yield of the adsorbed specie compared to its yield in an electromagnetically "inert" environment. Thus, the radiative yield of the state becomes

$$Y' = \gamma'_r \frac{|A(\omega',r)|^2}{\Gamma'}; \tag{4}$$

while the photochemical yield is reduced by the increased decay rate of the excited state

$$Y'_{pc} = \frac{\gamma'_{pc}}{\Gamma'}. \tag{5}$$

The essential physics of the electrodynamic interactions described for an isolated island remains even for the highly complex electromagnetic environment of the entire island film. In our modeling, we use the effective polarizability $\beta(\omega)$ to account for the effects of this complicated situation. The proximity of many neighboring islands, each with somewhat different shape, causes a substantial electromagnetic interaction among the electronic plasma resonances of the individual islands. This has the effect of broadening and shifting the resonance to lower energy than that of an isolated spheroid. Despite this complexity of the electrodynamics of the surface, the absorption spectrum $E(\omega)$ of the surface has proven to be an excellent characterization of the plasma resonances since it directly reflects the strength of electromagnetic fields within the islands of the film. The frequency dependence of β and E are then related (using the appropriate boundary conditions)

$$|\beta(\omega)|^2 \sim \frac{|\epsilon|^2 E(\omega)}{\omega\epsilon_2}, \tag{6}$$

where $\epsilon = \epsilon_1 + i\epsilon_2$ is the dielectric constant of the metal in the island. This characterization has led to prediction of the SERS excitation profile on an island film from the absorption of the film.[16] Since for silver and gold $|\epsilon|^2$ is a function which rises steeply with decreasing ω, $|\beta|^2$ shows resonant behavior similar to the absorption of the island film but with slower decrease at longer wavelengths.

B. Radiative yields and decay rates

A series of fluorescence emission spectra from RuTBP on different surfaces is shown in Fig. 1. While the spectra have been normalized to emphasize their spectral shifts, both intensity and spectral information reveal characteristics of the electrodynamics. On silver-island films on silica (Ag/SiO_2), the fluorescent intensity is enhanced by a factor of 1.7 over the intensity of the same molecular coverage on bare silica (SiO_2). This enhancement is intermediate between that measured for a molecule with a very high free quantum efficiency (Rhodamine 6G) and a molecule with a very low free quantum efficiency (basic Fuchsin).[4] On silver-island films on aluminum substrates (Ag/Al), the flat metal substrate quenches emission from all molecules between the islands; and RuTBP on this substrate shows an even lower fluorescent intensity. Since Ag/SiO_2 surfaces are about 40% silver and 60% silica, the emission from these films arises both from molecules near islands as well as from molecules in between islands. On Ag/Al, emission from molecules on the flat metal between islands is quenched and the observed emission arises only from molecules near islands; while on

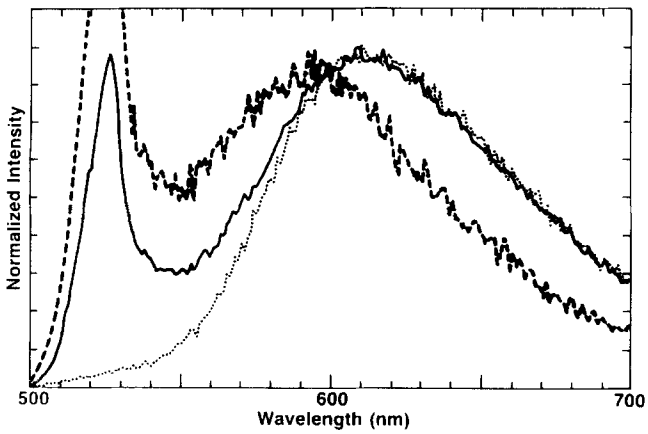

FIG. 1. Normalized fluorescence spectrum from RuTBP on (—) Ag/SiO_2; (- - -) Ag/Al; (···) SiO_2.

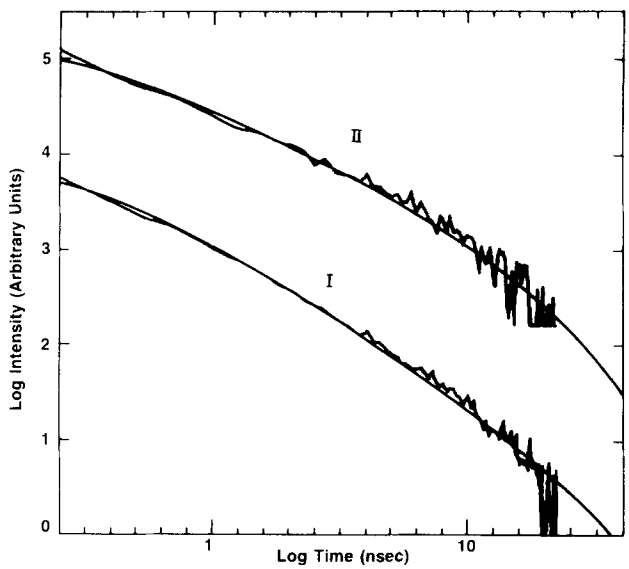

FIG. 2. Temporal decay of fluorescence of RuTBP (I) silver-island film with excitation at 488.0 nm. (II) Gold-island film with excitation at 457.9 nm. Emission detected at 600.0 nm. (—) theory for each case.

SiO_2, the emission is representative of that from molecules effectively separated large distances from any island. As seen in Fig. 1, the emission spectrum from molecules in these different spatial regions of the film show systematic shifts: emission from molecules near islands (i.e., emission from Ag/Al) is shifted to higher energy than emission from molecules far from islands (i.e., emission from SiO_2). Since coverages on all substrates are sufficiently low that no aggregation of RuTBP molecules is present, the observed spectral shifts do not arise from simple surface induced increases in the quantum yield of molecular aggregates (which have spectra shifted from that of the monomer) as has been previously observed.[6,19]

Our measurements of the fluorescence decay time and photochemical reaction rate on island films provide direct evidence of the increased decay rate of the excited state of a molecule near an island on the films. As seen in Fig. 2, the fluorescent decay measurements on RuTBP exhibit similar behavior to that found for the fluorescent decay of a rare earth chelate on silver-island films.[7] The exponential decay of RuTBP in solution ($\sim$200 ns) has been replaced by a nonexponential decay which occurs on a much shorter time scale when the molecule is on a silver-island film. The enhancement of the total intensity for the molecule on the island film clearly indicates that this increased decay rate is at least in part due to an enhanced radiative rate as opposed to an increase only in the nonradiative rate as would occur on a flat metal surface. As has been observed for another adsorbate,[9] the photochemical reaction rate of RuTBP is slower on Ag/SiO_2 than on SiO_2. This is another direct measurement of the surface-induced increase in the decay rates from the excited states of the adsorbate. Finally, the previously observed[4] enhancement of the fluorescence from a molecule such as basic Fuchsin where emission in the free state is quenched by very rapid ($\sim$10 ps) nonradiative processes shows that coupling to the plasma resonance can increase radiative decay rates even to the extent that they can successfully compete with these ultrafast molecular processes.

C. Temporal decay of fluorescence

While the shortening of the time scale of the decay is direct evidence of the surface-induced increase in the total decay rate, the nonexponential behavior seen in Fig. 2 results from the contributions of molecules at many distances from the islands and reflects the spatial variation in the coupling strength to the electronic plasma resonances. In order to probe the dependence of the shape of the decay curve on the tuning of the molecular state and the film plasma resonance, the decay measurements were made on different island films. Curve I of Fig. 2 shows the decay for molecules on Ag/SiO_2 using an excitation wavelength of 488.0 nm and an emission wavelength of 600.0 nm. Curve II on Fig. 2 shows the decay for molecules on a gold-island film using excitation and emission wavelengths of 457.9 and 600.0 nm, respectively.

The temporal decay of the fluorescence from RuTBP on island films (Fig. 2) can be quantitatively described by the model of the electrodynamic coupling. (The details of this model may be found in the Appendix.) Assuming exponential decay for the fluorescence of a molecule a fixed distance from an island, the time resolved emission is

$$\frac{dP_f}{dt} \propto \gamma_r' \frac{|A(\omega,r)|^2}{\Gamma} |A(\omega',r)|^2 e^{-\Gamma' t}. \tag{7}$$

The total signal from all molecules on the film is modeled by integrating the fluorescence of each molecule over a layer uniformly distributed in a disk about the spheroid

$$F(t) = N \int_b^{r_0} \frac{dP_f}{dt} d^2 r, \tag{8}$$

where N is the number of molecules per unit area and the lower limit of integration is the edge of the spheroid $r = b$. In the spirit of mean field models of island films, we assume that the molecules are dominated by the electrodynamic interactions with the nearest island with the effects of other islands accounted for by the polarizability $\beta(\omega)$ of the nearest island. Thus, the upper limit on the integral in Eq. (8) should be approximately one-half the distance between islands.

In Fig. 2, two limiting cases of our model are compared with the measured fluorescent decay of RuTBP on silver-

and gold-island films. In the first case, we assume that both the excitation and emission frequencies are within the plasma resonance of the film, and therefore, the effective polarizability $|\beta|^2$ takes on equal and large values at both frequencies. In the second case, we assume that only the emission frequency is within the plasma resonance; and therefore, the polarizability is much smaller at the excitation frequency than at the emission frequency. Our measurements of the absorption of the films and the excitation profile for SERS[16] suggest that the plasma resonance of the silver-island film does overlap both the excitation (488.0 nm) and emission (600.0 nm) wavelengths used in the experimental data in curve I of Fig. 2. Thus, this data should correspond to our model in the limit of large polarizability at both frequencies. In contrast, the plasma resonance of the gold-island film overlaps the emission frequency (600.0 nm) but not the excitation frequency (457.9 nm) used in the experimental data in curve II of Fig. 2. Thus, this data should correspond to our model in the limit of large polarizability at the emission frequency.

As shown in Fig. 2, we obtain excellent agreement between the modeled curves and the data from the two types of island films. Agreement between the model and the data is determined by using a least squares minimization of deviations with respect to the two adjustable parameters in the equations derived in our model [i.e., Eq. (A50) for the case of large polarizability at both frequencies and Eq. (A49) for the case of large polarizability at only the emission frequency]. These adjustable parameters represent scaling factors along the intensity and time axes. By varying these parameters, we find the best fit of *both* limiting cases of our model for *each* data set; the limiting case most appropriate to each data set is selected based on the smaller χ^2 (sum of the square of the deviations). For each data set χ^2 is reduced by roughly a factor of 2 by choosing the proper limiting case of the model. The shape of the lifetime for RuTBP on silver films is fit much better by the limit where both the excitation and emission frequencies match the island film resonance; while the shape of the lifetime on the gold film is fit much better by the other limit where only the emission frequency matches the island film resonance.

The time axis scaling factor is a function of the intrinsic properties of the metal and adsorbate as well as the structure of the film. For a sphere the scaling factor is

$$\Omega' = \frac{9\gamma_r'}{\epsilon_2^2}\left[1+\frac{1}{2}\epsilon_2\left(\frac{c}{b\omega'}\right)^3\right], \tag{9}$$

where c is the speed of light. Electron micrographs show that the islands on the gold and silver films are roughly circular in cross section and the same size. Thus, using the bulk dielectric constants of the metals,[25] we can predict a ratio for the scaling factors for our two experiments

$$\frac{\Omega'_{\mathrm{Ag}}}{\Omega'_{\mathrm{Au}}} = 0.61. \tag{10}$$

Our fitting procedure for the experiment yields a ratio of 0.42. This excellent agreement gives further credence to our modeling of these two limiting cases and provides strong evidence that the essential character of the electrodynamics of rough metal surface can be modeled by including only dipolar components of the response of the islands. This is in contrast to the nature of the electrodynamics at smooth metal or dielectric surfaces where higher order terms are essential.[24]

The lifetime of molecules nearest islands is dominated by the extremely rapid decay of the plasmon excitation of the film. Ω^{-1} is an upper limit on the shortest decay time of the molecules on the film. Our data analysis gives 5.6×10^{-10} and 3.5×10^{-10} s for Ω^{-1} on the silver and gold films, respectively, and represents an increase of about 500 over the free lifetime of the RuTBP. Estimates of the lifetime of the plasmon justify this extreme increase in the decay rate of the molecule via coupling to the islands. The plasmon lifetime has been calculated to be on the order of 2×10^{-14} s for an isolated spheroid.[15] Furthermore, if the localized plasmon is considered as a two-level system, the inverse of the homogeneous absorption width should correspond to the lifetime. We have observed that isolated clusters of islands as small as five islands show absorption resonances similar to those of complete films. Thus the observed absorption resonance of the film may be considered nearly homogeneous. The inverse of the 140 nm line width of our silver-island films is on the order of 7×10^{-16} s. These estimates indicate that the plasmon decay is indeed very rapid and justify the observed increase in the emission rate of RuTBP on these films.

D. Spectral shifts

As we have seen, the nonexponential decay of the fluorescence of RuTBP on the island films is a reflection of the distance dependence of the electromagnetic coupling between the molecules and the islands. To account for the shape of the decay, we must integrate over the spatial distribution of the molecules on the film. We can probe this spatial distribution, as well as the consequences of the variation in the coupling strength, more directly by taking advantage of the slightly different emission spectra observed in Fig. 1 for the molecules at different positions on the film. The combination of observations that molecules at different positions on the film (a) have different decay times and (b) show different emission spectra suggests that the shape of the fluorescent emission as a function of time after pulsed excitation also be studied.

The temporal development of the emission spectrum of RuTBP on Ag/SiO_2 is shown in Fig. 3. Due to the temporal resolution limitations of our measurement system, short time spectra cannot be independently resolved and early time curves represent contributions over an interval from zero time delay to some fixed time. For longer time, an explicit time interval is established for each spectrum. As the delay after pulsed excitation is increased, the ratio of resonance Raman scattered intensity (the sharp feature at 520 nm arises from a series of Raman lines unresolved by the spectrometer) to fluorescence decreases. Also the fluorescence spectrum shifts to longer wavelength as the spectrum develops. As seen in Fig. 4(a), the emission spectrum at short times after pulsed excitation is similar to the emission of molecules near islands under continuous excitation, i.e., emission from Ag/Al. Similarly, as seen in Fig. 4(b), the

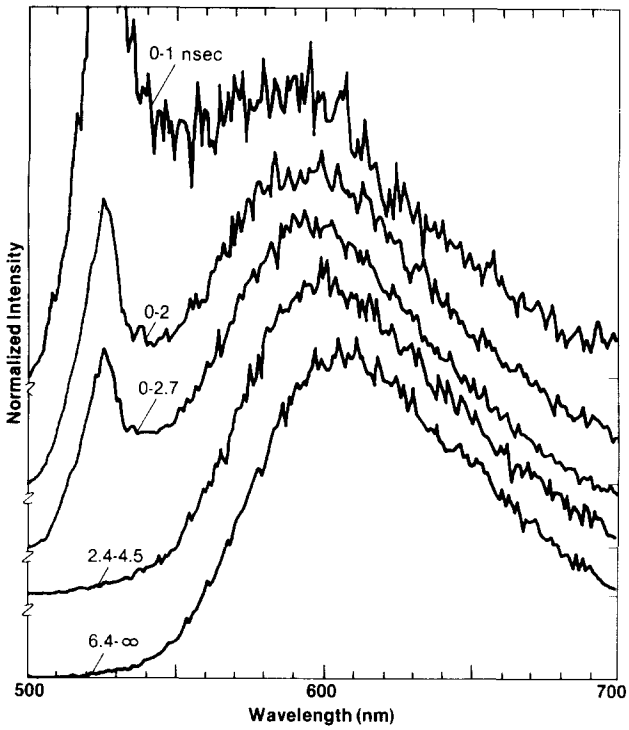

FIG. 3. Temporal evolution of normalized spectrum of RuTBP on silver-island film. Times marked on each curve represent the temporal window after pulsed excitation during which fluorescence is collected.

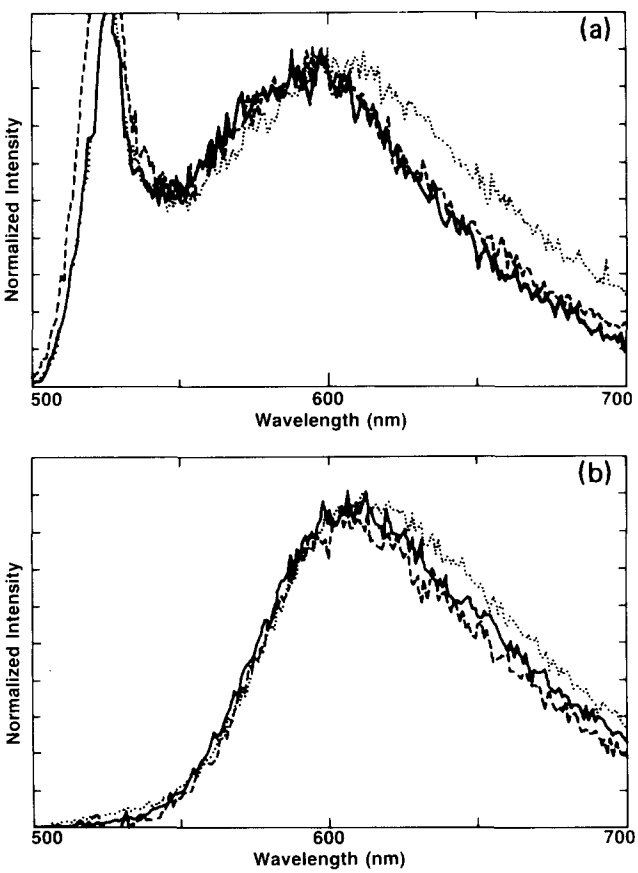

FIG. 4. (a) Normalized fluorescence spectrum from RuTBP: (—) 0–1.5 ns after pulsed excitation on Ag/SiO_2; (- - -) cw excitation on Ag/Al; (···) cw excitation after photochemical degradation on Ag/SiO_2. (b) Normalized fluorescence spectrum from RuTBP: (—) 6.4 ns after pulsed excitation on Ag/SiO_2; (- - -) removed by photochemical degradation on Ag/SiO_2; (···) cw excitation on bare SiO_2.

emission spectrum at longer times after pulsed excitation is similar to the emission of molecules unaffected by coupling to islands under continuous excitation, i.e., emission from bare SiO_2.

An additional probe of the spatial distribution of molecules on the island films is provided by the photochemical degradation experiments. As found for another absorbate,[9] not only is the photochemical reaction rate of RuTBP on a silver-island film slower than that for the molecule on a bare silica substrate; but, as shown on Fig. 5, the emission spectrum shows a progressive shift to longer wavelength in the following sequence: the spectrum after photochemical degradation to the spectrum before degradation to the spectrum lost in the degradation process (equal to the spectrum before minus the spectrum after degradation). This alteration of the fluorescence spectrum by the spatially inhomogeneous, surface-induced changes in the photochemical reaction rate is analogous to the photochemical hole burning in crystalline materials.[26] As can be observed from Fig. 4(a), those molecules which have faster photochemical reaction rates (i.e., those which stop fluorescing due to exposure to the intense laser radiation) give emission spectra similar to those on bare silica. These molecules are on the silica between the islands on the film and exhibit a photochemical reaction rate roughly equal to that on bare silica. The coupling between islands and these molecules does not substantially change the photochemical rate either through enhanced decay or enhanced pumping of exicted states of the molecule. In contrast, as shown in Fig. 5, some molecules on the film remain after exposure to intense laser radiation and thus have a slower photochemical degradation rate. As seen in Fig. 4(b), these molecules give spectra similar to that for RuTBP on silver islands on aluminum where only molecules very near islands can emit light. Here, despite the enhanced pumping of the excited states of the molecule, surface-induced increases in the radiative and nonradiative decay of the molecule dominate over branching into the photochemical channel; and thus, the degradation rate of these molecules is slower than that for molecules between the islands. Measurements of the enhancement of other optical processes on silver-island films indicate quantitatively that for molecules near islands, the

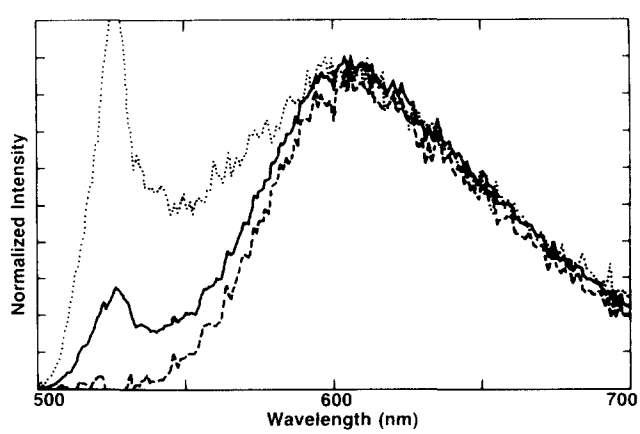

FIG. 5. Normalized fluorescence spectrum from RuTBP on Ag/SiO_2: (—) before photochemical degradation; (- - -) removed by photochemical degradation; (···) after photochemical degradation.

surface-induced increase in the nonradiative damping can dominate other decay channels and can counterbalance the enhancement in the pumping rate of the excited state.[4,9]

The origin of the spectral shifts observed in the emission of different subsets of molecules on island films is unclear. Experiments[4,8] and theory (Ref. 15 and the Appendix of this paper) indicate that the emission of molecules in the first layer directly on the surface of the islands is heavily damped and does not contribute significantly to the fluorescent emission from adsorbate coated island films. Therefore, the observed shifts are probably not due to simple differences in the local chemical environment between molecules bonded to the metal and silica surfaces of the film. Instead, the shifts may be a direct consequence of the electrodynamic interactions present on the film. In the increase in emission of a low quantum yield molecule[4] and the decrease in the photochemical degradation rate, we see evidence that the rapid surface-induced decay channels can compete successfully with photochemical and nonradiative processes which can depopulate thermally equilibrated vibrational states in an excited electronic manifold. However, the spectral shifts of molecules very near islands may indicate a successful competition of the surface-induced decay with the molecular processes (internal conversion) which produce this equilibrium of the population among these vibrational levels. This could produce the higher energy or "hot" fluorescence observed for the molecules very near islands.

Even if the strength of the coupling is insufficient to compete successfully with the internal conversion processes of the molecule, the frequency dependence of the surface-induced processes could be responsible for the observed shifts. The effective yield of each fluorescent transition connecting the thermalized lowest vibrational level of the excited electronic manifold to each vibrational level of the ground electronic manifold will be altered by the electrodynamic coupling at the frequency ω' of the transition. The fluorescence yield [Eq. (4)] has a frequency dependence which is related to the frequency dependence of the plasma resonance of the film [through $A(\omega,r)$] and the Frank-Condon factors connecting pairs of emitting states of the free molecule (through γ_r'). Therefore, the observed shape of the emission spectrum from the coated island film reflects both these frequency dependences. Thus, for the molecules nearest the islands, which experience the strongest coupling to the plasma resonance, the relative weighting of the emission from different pairs of states would be altered, changing the observed emission spectrum. In contrast, the molecules far from the islands, which experience weaker coupling, would exhibit a spectrum more reflective of the emission spectrum of the molecule in an electromagnetically inert environment. This explanation for the origin of the spectral shifts is supported by the result that the emission spectrum of RuTBP on gold-island films is shifted compared to the spectrum on silver-island films. Here the plasma resonance of the gold-island film is at lower energy than the free molecule absorption and emisison bands, and the emission spectrum of the coated film is shifted to lower energy than the spectrum on bare SiO_2. Therefore, the emission is weighted toward the film resonance whether it is at higher energy (silver-island films) or at lower energy (gold-island films) than the free molecular emission.

IV. SUMMARY

In this paper, we have described studies of delayed photophysical and photochemical processes of adsorbed molecules on island films. Our experiments have taken a unified approach to various aspects of the delayed optical processes. All measurements are made using a single adsorbate at roughly equal coverages on a number of substrates. Several aspects of the fluorescence of the molecule have been used to monitor the flow of electromagnetic energy during the optical processes experienced by adsorbates on rough metal surfaces. These aspects include: the magnitude and temporal decay of the intensity of the emission, the shape and temporal evolution of the spectrum of the emission, and the effects on the spectrum of a photochemical hole-burning process. The fluorescent intensity of RuTBP is increased on a silver-island film compared to that from the molecule on a silica surface; and the decay of that intensity becomes much more rapid and nonexponential. The photochemical degradation rate is also slowed. Systematic shifts in the emission spectrum are observed in three cases: (a) for the molecules on substrates designed to emphasize emission from different portions of the island film, (b) as the spectrum develops temporally after pulsed excitation, and (c) after photochemical degradation due to exposure to intense laser radiation. These shifts not only appear in each of the three cases but there are distinct resemblances between spectra produced when the different methods are used to explore similar electrodynamic regimes.

We have modeled our results with the electrodynamic picture which has successfully described various aspects of SERS and other optical processes on island films. Here, account of the molecular resonance and delayed nature of the processes has been included. This electrodynamic model is especially well suited to describe delayed processes on island films where chemical effects should be negligible. While simplified to make the problem tractable, our model highlights the essential physics of the situation: the dominantly dipole–dipole nature of the coupling between the adsorbate and the plasma resonance of the islands. The model predicts enhanced pumping rates of the excited states of the adsorbate and altered yields into various deexcitation channels due to surface-induced decay mechanisms. In addition, the model points out that an island film produces an inhomogeneous electromagnetic environment for the molecules on the film.

The comparison between our experimental results and the electrodynamic model indicates that this model provides an excellent description of delayed optical processes of adsorbates on island films. The temporal decay of the intensity of the fluorescence quantitatively follows the predictions of the model in two independent, limiting cases. From fitting of the data, we find that the coupling of the surface plasmon to the emitting state of the adsorbate can speed up the emission by over a factor of 500. Observed changes in effective quantum yield and photodegradation rate are then seen as a direct reflection of the predicted, rapid, surface-induced decay mechanisms.

The results of our three spectral measurements give a consistent picture of the distance dependence of the surface-induced changes in delayed photophysical and photochemical processes and they support the prediction of the electrodynamic model. Excited molecules nearest islands do decay most rapidly due to strong coupling to the ultrafast decay processes of the plasma resonances of the islands. This subset of molecules has a spectrum shifted to higher energy compared to the spectrum of the more weakly coupled molecules between islands. This systematic shift of emission spectra is not only seen as each experimental method probes the different subsets of molecules on the island film (Figs. 1, 3, and 5) but also as different experimental method probe the same subset of molecules (Fig. 4). There is a clear equivalence between molecules near islands, those removed most rapidly from the photochemical reactive state by surface-induced decay channels, and those with most rapid decay from the fluorescent emitting state. There is a similar equivalence between molecules between islands, those remaining in the photochemically reactive state longer, and those with slower decay from the fluorescent emitting state.

In conclusion, we have presented a detailed study of the consequences of the electrodynamic interactions with the electronic plasma resonances of a rough metal surface on the delayed photophysical and photochemical processes of adsorbed molecules. We have shown these interactions can have a profound effect: increasing the fluorescent emission decay rate, changing the shape of the spectral emission, and altering the rate of photochemical reactions on the surface. All of these effects have been interpreted in a consistent fashion by considering only the dipole–dipole coupling between the adsorbate and the plasma resonances of the islands. This essential dipolar character of the electrodynamics at rough metal surfaces sets these surfaces apart from flat metal or simple dielectric surfaces and is a fundamental contribution to the many unusual optical properties of rough metal surfaces.

APPENDIX

In this Appendix we describe some of the details of the electrodynamic model used to analyze our measurements of the temporal decay of fluorescence. The physical system consists of a set of metallic islands on a dielectric substrate which are covered by adsorbed molecules. The following idealized model is introduced in order to capture the essential physics of the problem. First, we consider one island which will be modeled as an oblate spheroid whose symmetry axis is perpendicular to the surface which is the xy plane. The molecules will be assumed to be uniformly distributed in the equatorial plane of the spheroid. The distance from the center of the spheroid to its tip along the symmetry axis is a and b is the radius of the equatorial circle. Since the spheroid is oblate, $a < b$. The incident laser field $\mathbf{E}_0$ is taken to be in the xy plane. We will treat the response of the spheroid as that of a point dipole. Higher order multipoles are relatively unimportant except in describing the field very near the spheroid surface, where theory[4,15] and experiments[8] show little of the observed fluorescent intensity is produced. The dipole assumption captures the essential character of the electrodynamic coupling between the molecule and the spheriod. Likewise, a given molecule will be treated as a point polarizable object. Let $\mathbf{r}$ denote the position of the molecule and let the spheroid be centered at the origin. We are assuming that the size of the spheroid-molecule system is small compared with the wavelength of light, so that only electric dipole radiation need be considered.

First we examine the decay channels open to a molecule in an excited state due to coupling to the spheroid dipole. The in-phase component of the dipole induced in the spheroid leads to an increase in the total emitting dipole of the system and thus produces an increase radiative decay rate. This decay rate is[15]

$$\Gamma_{\parallel}^{R} = \frac{|A_{\parallel}|^2}{|1-\Delta_{\parallel}|^2}\gamma_r\,, \tag{A1}$$

$$\Gamma_{\perp}^{R} = \frac{|A_{\perp}|^2}{|1-\Delta_{\perp}^2|}\gamma_r\,, \tag{A2}$$

for molecules oriented parallel and perpendicular to the radial vector joining the center of the spheroid and the molecule. γ_r is the radiative rate of the free molecule. The enhancement factors are

$$A_{\parallel} = 1 + \frac{2\alpha(\omega)\beta(\omega)}{r^3}\,, \tag{A3}$$

$$A_{\perp} = 1 - \frac{\alpha(\omega)\beta(\omega)}{r^3} \tag{A4}$$

and

$$\Delta_{\parallel} = \frac{4\alpha(\omega)\beta(\omega)}{r^6}\,, \tag{A5}$$

$$\Delta_{\perp} = \frac{\alpha(\omega)\beta(\omega)}{r^6}\,, \tag{A6}$$

where $\alpha(\omega)$ is the frequency dependent polarizability of the molecule (assumed isotropic for a free molecule) and $\beta(\omega)$ is the frequency dependent effective polarizability of the spheroid (which is isotropic in the xy plane). Since the molecular polarizability is always very small and—as we shall see—β is never much greater than the spheroid volume, $|\Delta_{\parallel}|$ and $|\Delta_{\perp}|$ can be neglected for all r under consideration.

The oscillating dipole of the excited molecule also induces an out-of-phase component in the dipolar response in the spheroid. This component beats against the local field and results in a surface-induced nonradiative dissipation of energy. The nonradiative rates for this process are[15]

$$\Gamma_{\parallel}^{NR} = \frac{2|\boldsymbol{\mu}_0|^2}{r^6}\,\mathrm{Im}\,\beta, \tag{A8}$$

$$\Gamma_{\perp}^{NR} = \frac{|\boldsymbol{\mu}_0|^2}{r^6}\,\mathrm{Im}\,\beta, \tag{A9}$$

where $\boldsymbol{\mu}_0$ is the molecular dipole. The total decay rate of any state of the system can now be written. For the parallel orientation,

$$\begin{aligned}\Gamma_{\parallel} &= \gamma_{nr} + \Gamma_{\parallel}^{R} + \Gamma_{\parallel}^{NR} \\ &= \gamma + \gamma_r(|A_{\parallel}|^2 - 1) + \frac{2|\boldsymbol{\mu}_0|^2}{r^6}\,\mathrm{Im}\,\beta,\end{aligned} \tag{A10}$$

where γ and γ_{nr} are the total and nonradiative decay rates of

the free molecular, respectively. (For simplicity in this Appendix, we neglect photochemical pathways available to the molecule.) Similarly, for the perpendicular orientation,

$$\Gamma_\perp = \gamma + \gamma_r(|A_\perp|^2 - 1) + \frac{|\mu_0|^2}{2r^6}\,\mathrm{Im}\,\beta. \tag{A11}$$

The fluorescence process consists of absorption and reradiation of a photon by the system. Reradiation occurs after a rapid sequence of vibrational relaxation steps in the excited electronic manifold which both break the coherence between absorption and emission processes and shift the photon frequency from ω, the absorption frequency, to ω' the emission frequency. (Throughout the paper, frequency dependent quantities evaluated at ω' will be denoted by primes while those evaluated at ω will be denoted without primes.) After this rapid internal conversion within the excited electronic manifold, the system further relaxes to the ground electronic state either radiatively or nonradiatively. The quantum yield Y' is the ratio of the radiative to total decay rates for this relaxation to the ground state. Since the emission dipole of the molecule $\boldsymbol{\mu}_0'$ is not in general aligned on either the parallel or perpendicular directions, the molecule will excite both parallel and perpendicular responses in the spheroid. Thus, in writing the quantum yield, we use a weighted average of the responses

$$Y' = \gamma_r'\left[\frac{\hat{\mu}_0'^{*}\cdot\mathsf{R}_\parallel\cdot\hat{\mu}_0'\,|A_\parallel'|^2}{\Gamma_\parallel'} + \frac{\hat{\mu}_0'^{*}\cdot\mathsf{R}_\perp\cdot\hat{\mu}_0'\,|A_\perp'|^2}{\Gamma_\perp'}\right], \tag{A12}$$

where

$$\mathsf{R}_\parallel = \hat{r}\hat{r} \tag{A13}$$

and

$$\mathsf{R}_\perp = \mathsf{I} - \hat{r}\hat{r} \tag{A14}$$

are operators which project onto the parallel and perpendicular directions, respectively, I is the identity operation, and $\hat{\mu}_0'$ is the unit vector along $\boldsymbol{\mu}_0'$.

Let us now turn our attention to the absorption process. The local field at the spheroid is

$$\mathbf{E}_s = \mathbf{E}_0 + \mathsf{M}\cdot\boldsymbol{\mu}, \tag{A15}$$

and the local field at the molecule is

$$\mathbf{E}_m = \mathbf{E}_0 + \mathsf{M}\cdot\mathbf{p}, \tag{A16}$$

where M is the dipole operator

$$\mathsf{M} = \frac{2\mathsf{R}_\parallel - \mathsf{R}_\perp}{r^3}. \tag{A17}$$

The molecular dipole is

$$\boldsymbol{\mu} = \boldsymbol{\alpha}\cdot\mathbf{E}_m, \tag{A18}$$

and the spheroid's dipole is

$$\mathbf{p} = \beta\,\mathbf{E}_s. \tag{A19}$$

Even though α is assumed isotropic for the free molecule, we shall see that it takes on different values in the parallel and perpendicular directions near the spheroid. Solving Eqs. (A15)–(A19) yields

$$\boldsymbol{\mu} = \left(\alpha_\parallel\frac{A_\parallel\mathsf{R}_\parallel}{1-\Delta_\parallel} + \alpha_\perp\frac{A_\perp\mathsf{R}_\perp}{1-\Delta_\perp}\right)\cdot\mathbf{E}_0. \tag{A20}$$

The square of the molecular dipole moment is

$$|\boldsymbol{\mu}|^2 = \mathbf{E}_0^{*}\cdot\mathsf{R}_\parallel\cdot\mathbf{E}_0\left|\frac{A_\parallel}{1-\Delta_\parallel}\right|^2|\alpha_\parallel|^2 + \mathbf{E}_0^{*}\cdot\mathsf{R}_\perp\cdot\mathbf{E}_0\left|\frac{A_\perp}{1-\Delta_\perp}\right|^2|\alpha_\perp|^2. \tag{A21}$$

In deriving Eq. (A21), classical radiation theory has been used. In quantum mechanics, the quantity $|\boldsymbol{\mu}|^2$ is to be interpreted as a product of the square of the transition moment $|\mu_0|^2$ and the excitation probability P. Thus,

$$P = \left|\frac{1}{\mu_0}\right|^2\mathbf{E}_0^{*}\cdot\mathsf{R}_\parallel\cdot\mathbf{E}_0\left|\frac{A_\parallel}{1-\Delta_\parallel}\right|^2|\alpha_\parallel|^2 + \mathbf{E}_0^{*}\cdot\mathsf{R}_\perp\cdot\mathbf{E}_0\left|\frac{A_\perp}{1-\Delta_\perp}\right|^2|\alpha_\perp|^2. \tag{A22}$$

Note that the same amplification factors that were found associated with enhanced radiative decay rates in Eqs. (A1) and (A2) also appear in the expression for the absorption probability. Thus, the probability of absorbing a photon is enhanced by the factor $|A/(1-\Delta)|^2$ due to the enhanced local field at the position of the molecule. As before, we will neglect the Δ terms in the demoninators.

Further progress is made by introducing a microscopic model for the molecular polarizabilities

$$\alpha_\parallel = \frac{|\mu_0|^2}{4}\frac{1}{\omega_0 - \omega - i\dfrac{\Gamma_\parallel}{2}}, \tag{A23}$$

$$\alpha_\perp = \frac{|\mu_0|^2}{4}\frac{1}{\omega_0 - \omega - i\dfrac{\Gamma_\perp}{2}}, \tag{A24}$$

where ω_0 is the molecular electronic resonance frequency associated with the absorption process and $i = \sqrt{-1}$. The width of the state Γ is increased over the width of the free molecule due to the surface-induced radiative and nonradiative processes. In Eqs. (A23) and (A24), we have set $h = 1$ for convenience. Equation (A22) may now be written as

$$P = \frac{|\mu_0|^2}{16}\left[\mathbf{E}_0^{*}\cdot\mathsf{R}_\parallel\cdot\mathbf{E}_0\left|\frac{A_\parallel}{\omega_0 - \omega - i\dfrac{\Gamma_\parallel}{2}}\right|^2 + \mathbf{E}_0^{*}\cdot\mathsf{R}_\perp\cdot\mathbf{E}_0^{*}\left|\frac{A_\perp}{\omega_0 - \omega - i\dfrac{\Gamma_\perp}{2}}\right|^2\right]. \tag{A25}$$

In large molecules, an inhomogeneous distribution of resonance energies exists due to the many vibrational and rotational levels for a given excited electronic state. While some of this distribution is due to site inhomogeneity, the primary source is the high density of energy levels itself. Thus P must be averaged over the inhomogeneous distribution $F(\omega_0)$. For simplicity's sake, we take $F(\omega_0)$ to be a Lorentzian function centered around a frequency ω_m with a width parameter δ. Thus,

$$\langle P\rangle = \frac{1}{2\pi}\int_{-\infty}^{\infty} d\omega_0\,\frac{\delta}{(\omega_0 - \omega_m)^2 + (\delta/2)^2}\,P. \tag{A26}$$

If the inhomogenous width δ is much larger than the homogeneous widths $\Gamma_\perp$ and $\Gamma_\parallel$, then Eq. (A26) reduces to

$$\langle P\rangle = \frac{|\mu_0|^2}{4\delta}\,\mathbf{E}_0^*\cdot\left[\frac{|A_\perp|^2}{\Gamma_\perp}\,\mathsf{R}_\perp + \frac{|A_\parallel|^2}{\Gamma_\parallel}\,\mathsf{R}_\parallel\right]\cdot\mathbf{E}_0 . \quad \text{(A27)}$$

Equation (A27) represents the probability for absorption of a photon by the molecule.

The fluorescence probability is obtained by multiplying the absorption probability by the emission yield. Then

$$\begin{aligned} P_F &= \langle P\rangle\, Y' \\ &= \frac{|\mu_0|^2}{4\delta}\,\gamma_r'\left[\frac{|A_\perp|^2}{\Gamma_\perp}\,\mathbf{E}_0^*\cdot\mathsf{R}_\perp\cdot\mathbf{E}_0 + \frac{|A_\parallel|^2}{\Gamma_\parallel}\,\mathbf{E}_0^*\cdot\mathsf{R}_\parallel\cdot\mathbf{E}_0\right] \\ &\quad\times\left[\frac{|A_\perp'|^2}{\Gamma_\perp'}\,\hat{\mu}_0'\cdot\mathsf{R}_\perp\cdot\hat{\mu}_0' + \frac{|A_\parallel'|^2}{\Gamma_\parallel'}\,\hat{\mu}_0'^*\cdot\mathsf{R}_\parallel\cdot\hat{\mu}_0'\right] . \end{aligned} \quad \text{(A28)}$$

Now we consider the time-resolved emission instead of the total emission. An exponential decay of the fluorescence from the molecule/island system is expected, i.e., for the perpendicular dipole to decay as $\exp(-\Gamma_\perp' t)$ and for the parallel dipole to decay as $\exp(-\Gamma_\parallel' t)$. Since

$$\int_0^\infty dt\,\exp(-\Gamma' t) = \Gamma'^{-1}, \quad \text{(A29)}$$

a normalization factor for each term in the quantum yield must be used. The time-resolved fluorescence emission is defined as

$$\begin{aligned} \frac{dP_F}{dt} &= \frac{|\mu_0|^2}{4\delta}\,\gamma_r'\left[\frac{|A_\perp|^2}{\Gamma_\perp}\,\mathbf{E}_0^*\cdot\mathsf{R}_\perp\cdot\mathbf{E}_0 + \frac{|A_\parallel|^2}{\Gamma_\parallel}\,\mathbf{E}_0^*\cdot\mathsf{R}_\parallel\cdot\mathbf{E}_0\right] \\ &\quad\times\left[\,|A_\perp'|^2\,\hat{\mu}_0'^*\cdot\mathsf{R}_\perp\cdot\hat{\mu}_0'\,e^{-\Gamma_\perp' t} + |A_\parallel'|^2\hat{\mu}_0'^*\cdot\mathsf{R}_\parallel\cdot\hat{\mu}_0' e^{-\Gamma_\parallel' t}\right] . \end{aligned} \quad \text{(A30)}$$

Physically $[(dP_F/dt)\,dt]$ is the fluorescence signal appearing between times t and $t+dt$.

Equation (A30) represents the fluorescence signal from one molecule a distance r from the center of the spheroid. Let us now assume that the xy plane has a density of N molecules per unit area. Since the density of molecules in our experiments is so low, no concentration quenching is seen and we can safely neglect intermolecular effects and only consider the island-molecule interaction. Then the net fluorescence signal is

$$F(t) = N\int \frac{dP_F}{dt}\,d^2r. \quad \text{(A31)}$$

Removing a prefactor which is independent of t and $\mathbf{r}$:

$$F(t) = \frac{|\mu_0|^2}{4\delta}\,\gamma_r'\,|\mathbf{E}_0|^2 T_F(t,r), \quad \text{(A32)}$$

where

$$\begin{aligned} T_F(t,r) &= \int_b^\infty r dr\int_0^{2\pi} d\phi \\ &\quad\times\left[\frac{|A_\parallel|^2}{\Gamma_\parallel}\,\hat{E}_0^*\cdot\mathsf{R}_\parallel\cdot\hat{E}_0 + \frac{|A_\perp|^2}{\Gamma_\perp}\,\hat{E}_0^*\cdot\mathsf{R}_\perp\cdot\hat{E}_0\right] \\ &\quad\times\left[\,|A_\parallel'|^2\hat{\mu}_0'^*\cdot\mathsf{R}_\parallel\cdot\hat{\mu}_0'\,e^{-\Gamma_\parallel' t} + |A_\perp'|^2\hat{\mu}_0'^*\cdot\mathsf{R}_\perp\cdot\hat{\mu}_0' e^{-\Gamma_\perp' t}\right] . \end{aligned} \quad \text{(A33)}$$

Equation (A33) still exhibits dependence on the relative orientations of the molecular emission dipole $\boldsymbol{\mu}_0'$, the applied electric field $\mathbf{E}_0$, and the position vector $\mathbf{r}$. Included in Eq. (A33) are terms of the form

$$T_1 = \hat{E}_0^*\cdot\mathsf{R}_\perp\cdot\hat{E}_0\,\hat{\mu}_0'\cdot\mathsf{R}_\perp\cdot\hat{\mu}_0, \quad \text{(A34a)}$$

$$T_2 = \hat{E}_0^*\cdot\mathsf{R}_\perp\cdot\hat{E}_0\,\hat{\mu}_0'^*\cdot\mathsf{R}_\parallel\cdot\hat{\mu}_0', \quad \text{(A34b)}$$

$$T_3 = \hat{E}_0^*\cdot\mathsf{R}_\parallel\cdot\hat{E}_0\,\hat{\mu}_0'\cdot\mathsf{R}_\perp\cdot\hat{\mu}_0', \quad \text{(A34c)}$$

$$T_4 = \hat{E}_0^*\cdot\mathsf{R}_\parallel\cdot\hat{E}_0\,\hat{\mu}_0'\cdot\mathsf{R}_\parallel\cdot\hat{\mu}_0', \quad \text{(A34d)}$$

Averaging these terms over all directions in the xy plane gives

$$\langle T_1\rangle = \langle T_4\rangle = \tfrac{1}{8}\left[1 + 2(\hat{\mu}_0'\cdot\hat{E}_0)^2\right], \quad \text{(A35a)}$$

$$\langle T_2\rangle = \langle T_3\rangle = \tfrac{1}{8}\left[3 - 2(\hat{\mu}_0'\cdot\hat{E}_0)^2\right] \quad \text{(A35b)}$$

Therefore,

$$\begin{aligned} T_F(t,r) = \frac{2\pi}{8}\int_b^\infty dr\,r\Bigg[&|A_\perp'|^2 e^{-\Gamma_\perp' t}\left(\frac{|A_\perp|^2}{\Gamma_\perp}(1+2\cos^2\psi) + \frac{|A_\parallel|^2}{\Gamma_\parallel}(3-2\cos^2\psi)\right) \\ &+ |A_\parallel'|^2 e^{-\Gamma_\parallel' t}\left(\frac{|A_\perp|^2}{\Gamma_\perp}(3-2\cos^2\psi) + \frac{|A_\parallel|^2}{\Gamma_\parallel}(1+2\cos^2\psi)\right)\Bigg], \end{aligned} \quad \text{(A36)}$$

where $\cos\psi = \hat{\mu}_0'\cdot\hat{E}_0$. For dye molecules, $\hat{\mu}_0'$ and $\hat{E}_0$ would be correlated due to the fixed angular relation between the absorption dipole and emission dipole of the thermalized state of the molecule. As a simplifying assumption, let these quantities be uncorrelated, then $\langle\cos^2\psi\rangle = \frac{1}{2}$. (The subsequent deviation can be carried through without this assumption with no change in the essential properties of the final result.) Then

$$\begin{aligned} T_F(t,r) = \frac{\pi}{2}\int_b^\infty dr\,r\,(&|A_\perp'|^2 e^{-\Gamma_\perp' t} + |A_\parallel'|^2 e^{-\Gamma_\parallel' t}) \\ &\times\left(\frac{|A_\perp|^2}{\Gamma_\perp} + \frac{|A_\parallel|^2}{\Gamma_\parallel}\right). \end{aligned} \quad \text{(A37)}$$

The shape of the curve describing the temporal decay of the fluorescent signal will depend on whether the excitation and/or emission frequencies are within the resonance of the spheroid. The conditions for resonance of the spheroid are found by examining the polarizability of the spheroid[15]

$$\beta(\omega) = \frac{2f^3}{3}\,\frac{\xi_0[1-\epsilon(\omega)]}{\epsilon(\omega)Q_1^{(1)}(\xi_0)P_1^{(1)\prime}(\xi_0) - P_1^{(1)}(\xi_0)Q_1^{(1)\prime}(\xi_0)}, \quad \text{(A38)}$$

where $f = (a^2-b^2)^{1/2}$ and $\xi_0 = a/f$, and $P_1^{(1)}$ and $Q_1^{(1)}$ are, respectively, the associated Legendre functions of the first and second kind, and $P_1^{(1)\prime}$ and $Q_1^{(1)\prime}$ are their derivatives with respect to their arguments. $\epsilon(\omega) = \epsilon_1 + i\epsilon_2$ is the complex dielectric constant of the material in the spheroid. For the oblate case considered here, appropriate analytic continu-

ation of Eq. (A38) must be made. The corresponding formula for a sphere of radius b is

$$\beta(\omega) = \frac{\epsilon(\omega) - 1}{\epsilon(\omega) + 2} b^3. \tag{A39}$$

The resonance condition for the spheroid is

$$\mathrm{Re}\,\epsilon(\omega) Q_1^{(1)}(\xi_0) P_1^{(1)'}(\xi_0) - P_1^{(1)}(\xi_0) Q_1^{(1)'}(\xi_0) = 0. \tag{A40}$$

At resonance, β reduces to

$$\beta \rightarrow \frac{-2if^3}{3} \frac{[1 - \epsilon(\omega)]}{\epsilon_2(\omega) Q_1'(\xi_0)}. \tag{A41}$$

For a sphere, Eq. (A40) becomes

$$\mathrm{Re}\,\epsilon(\omega) = -2, \tag{A42}$$

and Eq. (A41) becomes

$$\beta \rightarrow -i \frac{[\epsilon(\omega) - 1] b^3}{\epsilon_2(\omega)}. \tag{A43}$$

First, we examine the case where the excitation is not tuned to the spheroid resonance but the emission is. To model the off-resonance behavior, we assume the excitation frequency is in the range where the imaginary part of the dielectric constant of the metal spheroid is large due to the excitation of the interband transitions. Then $\beta(\omega) \rightarrow b^3$, where b is a characteristic length of the spheroid, e.g., the radius for an equivalent sphere. Since β is not resonant and large at the absorption frequency, we assume that the absorption width of the molecule γ is not substantially altered by the nonresonant excitation of the spheroid. Then $\Gamma_\perp = \Gamma_\parallel = \gamma$. To model the on-resonance condition, we assume that the real part of the dielectric constant of the spheroid satisfies Eq. (A40) and the damping of the resonance by the imaginary part is quite small. Then β' is given by Eq. (A41) which may be written in the general form $\beta' = (ib^3 d/\epsilon_2)$, where d is a dimensionless constant of order unity and depending on the aspect ratio of the spheroid. Since β' at this frequency is resonant and thus large, we assume that surface terms Γ' dominate the molecular rate γ'. (Experimentally we see direct evidence that the surface-induced rate is considerably faster than the free molecule decay rate.) Then

$$\Gamma_\parallel' \rightarrow \frac{1}{r^6}(4|\beta'|^2 + 2|\mu_0'|^2 \,\mathrm{Im}\,\beta'), \tag{A44}$$

$$\Gamma_\parallel' \rightarrow \frac{1}{r^6}(|\beta'|^2 + \tfrac{1}{2}|\mu_0'|^2 \,\mathrm{Im}\,\beta') = \tfrac{1}{4}\Gamma_\parallel'. \tag{A45}$$

Thus, letting $x = r/b$, we obtain

$$T_F(t,r) = T_0 \int_1^\infty \frac{dx}{x^5}\left(2 + \frac{2}{x^3} + \frac{5}{x^6}\right) \times \left(e^{-\frac{\Omega' t}{x^6}} + 4e^{-\frac{4\Omega' t}{x^6}}\right), \tag{A46}$$

where

$$\Omega' = |\beta'|^2 + \tfrac{1}{2}|\mu_0'|^2 \,\mathrm{Im}\,\beta'. \tag{A47}$$

The constant Ω' scales the time axis of the predicted fluorescence decay and T_0 is a constant prefactor. For a sphere, Ω' simplifies to

$$\Omega' = \frac{6|\mu_0'|^2}{4\epsilon_2 b^3} + \frac{9\gamma_r'}{\epsilon_2^2}. \tag{A48}$$

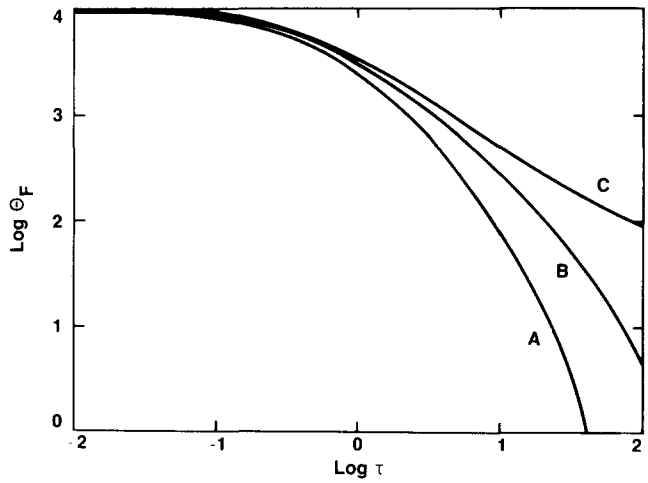

FIG. 6. Prediction of model for temporal decay of fluorescence when only the emission frequency is on resonance. Interisland spacing equal to: (A) 1.5 times the particle radius (B) three times the radius, and (C) five times the radius.

The single particle expression [Eq. (A46)] must be applied to the situation of the sample which can be represented as a collection of spheroids. In the spirit of a mean field approximation, we assume that the electrodynamics of each molecule is dominated by the nearest island with island–island effects accounted for in $\beta(\omega)$ of that nearest island. Thus, an upper limit for the integral in Eq. (A46) should be roughly one half the distance between islands or r_0. If $y = 1/x^6$, then the temporal behavior of the fluorescence of the sample is

$$\theta_F(\tau) = \int_{y_0}^1 \frac{dy}{y^{1/3}}[2 + 2\sqrt{y} + 5y] \times (e^{-\tau y} + 4e^{-4\tau y}), \tag{A49}$$

where $\tau = \Omega' t$ and $y_0 = b/r_0$. The quantity $\theta_F(\tau)$ is simply proportional to $T_F(t,r)$.

A graph of $\theta_F(\tau)$ vs τ is presented in Fig. 6. Several values of the parameter r_0 are chosen. The profile is flat for small times and falls off in a power law manner for long times. The power law behavior arises because of the integral

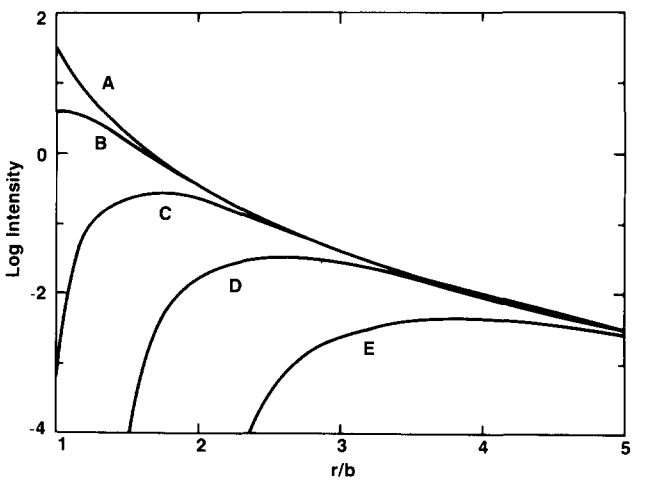

FIG. 7. Prediction of model for differential contribution to total fluorescence signal vs radius of annular ring of molecules. Curve (A), $\tau = 0.1$; (B) $\tau = 1$; (C) $\tau = 10$; (D) $\tau = 100$; (E) $\tau = 1000$.

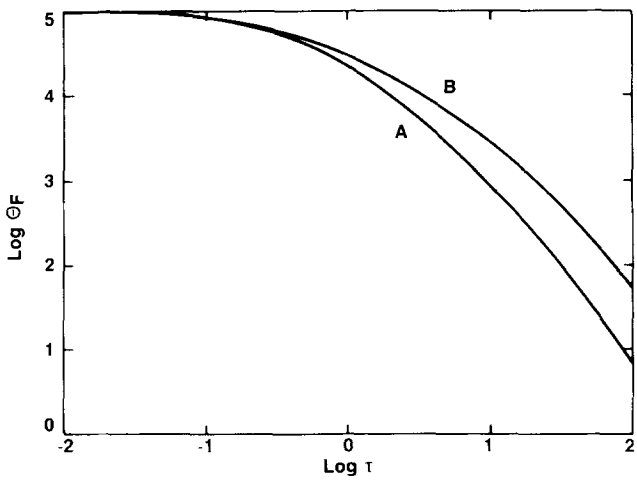

FIG. 8. Prediction of model for temporal decay of fluorescence for (A) both excitation and emission wavelengths on resonance and (B) only the emission frequency on resonance.

of exponential time decays over an inhomogeneous distribution of decay rates. Those molecules lying close to the island decay quickly, while those molecules which are more distant decay slowly. The effect of introducing a nonzero y_0 parameter is to put a limit on how far a molecule may be from the island (the interisland spacing). Thus it tends to diminish the long time behavior.

Figure 7 shows the differential contribution arising from a given ring of molecules which lie a distance $x\,(=r/b)$ from the origin. Curves are drawn for various values of the scaled time τ. For small τ the major contribution arises from $x \approx 1$, i.e., for molecules near the island. As time increases the peak contribution shifts towards larger r values. The quantity that is actually plotted is the integrand of Eq. (A49).

If both the excitation and emission frequencies are within the resonance of the spheroid, then the temporal decay will have a different shape. In Eq. (A36) $|A_\perp|^2$ and $|A_\parallel|^2$ will then both vary as $(b/r)^6$ and in place of Eq. (A49) we find

$$\tilde{\theta}_F(\tau) = \int_{y_0}^{1} dy\, y^{2/3}(e^{-\tau y} + 4e^{-4\tau y}). \tag{A50}$$

A plot of $\tilde{\theta}_F(\tau)$ is presented in Fig. 8 for the case of $y = 1/2$ and is compared with a similar plot for θ_F for $y_0 = 1/2$. The power law falloff is different in two cases.

[1] A recent review, see *Surface Enhanced Raman Scattering*, edited by R. K. Chang and T. E. Furtak (Plenum, New York, 1982).
[2] S. Garoff, D. A. Weitz, T. J. Gramila, and C. D. Hanson, Opt. Lett. **6**, 245 (1981).
[3] H. G. Craighead and A. M. Glass, Opt. Lett. **6**, 248 (1981).
[4] D. A. Weitz, S. Garoff, J. I. Gersten, and A. Nitzan, J. Chem. Phys. **78**, 5324 (1983).
[5] A. M. Glass, P. F. Liao, J. G. Bergman, and D.H. Olson, Opt. Lett. **5**, 368 (1980).
[6] G. Ritchie and E. Burstein, Phys. Rev. B **24**, 4843 (1981).
[7] D. A. Weitz, S. Garoff, C. D. Hanson, and T. J. Gramila, Opt. Lett. **7**, 89 (1982).
[8] A. Wokaun, H. P. Lutz, A. P. King, U. P. Wild, and R. R. Ernst, J. Chem. Phys. **29**, 509 (1983).
[9] S. Garoff, D. A. Weitz, and M. S. Alvarez, Chem. Phys. Lett. **93**, 283 (1982).
[10] M. Moskowitz and D. P. DeLella, Ref. 1, p. 243.
[11] A. Wokaun, J. G. Bergman, J. P. Heritage, A. M. Glass, P. F. Liao, and D. H. Olson, Phys. Rev. B **24**, 849 (1981).
[12] C. K. Chen, T. F. Heinz, D. Ricard, and Y. R. Shen, Phys. Rev. B **27**, 1965 (1983).
[13] D. S. Chemla, J. P. Heritage, P. F. Liao, and E. D. Isaacs, Phys. Rev. B **27**, 4553 (1983).
[14] J. I. Gersten and A. Nitzan, J. Chem. Phys. **73**, 3023 (1980).
[15] J. I. Gersten and A. Nitzan, J. Chem. Phys. **75**, 1139 (1980).
[16] D. A. Weitz, S. Garoff, and T. J. Gramila, Opt. Lett. **7**, 168 (1982).
[17] S. L. McCarthy, J. Vac. Sci. Technol. **13**, 135 (1976).
[18] T. S. Yamaguchi, S. Yashida, and A. Kimbara, Thin Solid Films **21**, 173 (1974).
[19] S. Garoff, R. B. Stephens, C. D. Hanson, and G. K. Sorenson, Opt. Commun. **41**, 257 (1982).
[20] S. Anderson, K. R. Seddon, R. D. Wright, and A. T. Cocks, Chem. Phys. Lett. **21**, 220 (1980).
[21] J. V. Caspar and T. J. Meyer, J. Am. Chem. Soc. **105**, 5583 (1983).
[22] K. G. Spears, L. E. Cramer, and L. D. Hoffland, Rev. Sci. Instrum. **49**, 255 (1974).
[23] P. R. VanDuyne, D. L. Jeanmaire, and D. F. Shriver, Anal. Chem. **46**, 213 (1974).
[24] R. R. Chance, A. Prock, and R. Silbey, Adv. Chem. Phys. **37**, 1 (1978).
[25] *Physics Data: Optical Properties of Metals*, edited by J. H. Weaver, C. Krafka, D. W. Lynch, and E. E. Koch (Fachsinformations Centrum, Karlsruhe, 1981), Vol. 1, pp. 46 and 59.
[26] S. Voelker, R. M. Macfarlane, A. Z. Genack, H. P. Tromsdorff, and J. H. vander Waals, J. Chem. Phys. **67**, 1759 (1977).